Nonlinear dynamics of cell migration in anisotropic microenvironment

Yanping Liu(刘艳平), Da He(何达), Yang Jiao(焦阳), Guoqiang Li(李国强), Yu Zheng(郑钰), Qihui Fan(樊琪慧), Gao Wang(王高), Jingru Yao(姚静如), Guo Chen(陈果), Silong Lou(娄四龙), and Liyu Liu(刘雳宇)

Citation: Chin. Phys. B, 2021, 30 (**9**): 090505. DOI: 10.1088/1674-1056/ac11d5
Journal homepage: http://cpb.iphy.ac.cn; http://iopscience.iop.org/cpb

What follows is a list of articles you may be interested in

Migration and shape of cells on different interfaces

Xiaochen Wang(王晓晨), Qihui Fan(樊琪慧), and Fangfu Ye(叶方富)
Chin. Phys. B, 2021, 30 (**9**): 090502. DOI: 10.1088/1674-1056/abf557

Stationary response of colored noise excited vibro-impact system

Jian-Long Wang(王剑龙), Xiao-Lei Leng(冷小磊), and Xian-Bin Liu(刘先斌)
Chin. Phys. B, 2021, 30 (**6**): 060501. DOI: 10.1088/1674-1056/abf12a

Directed transport of coupled Brownian motors in a two-dimensional traveling-wave potential

Wei-Xia Wu(吴魏霞), Zhi-Gang Zheng(郑志刚), Yan-Li Song(宋艳丽), Ying-Rong Han(韩英荣), Zhi-Cheng Sun(孙志成), Chen-Pu Li(李晨璞)
Chin. Phys. B, 2020, 29 (**9**): 090503. DOI: 10.1088/1674-1056/ab99b7

Stochastic bifurcations of generalized Duffing-van der Pol system with fractional derivative under colored noise

Wei Li(李伟), Mei-Ting Zhang(张美婷), Jun-Feng Zhao(赵俊锋)
Chin. Phys. B, 2017, 26 (**9**): 090501. DOI: 10.1088/1674-1056/26/9/090501

Hysteresis-induced bifurcation and chaos in a magneto-rheological suspension system under external excitation

Hailong Zhang(张海龙), Enrong Wang(王恩荣), Fuhong Min(闵富红), Ning Zhang(张宁)
Chin. Phys. B, 2016, 25 (**3**): 030503. DOI: 10.1088/1674-1056/25/3/030503

Nonlinear dynamics of cell migration in anisotropic microenvironment*

Yanping Liu(刘艳平)[1,†], Da He(何达)[2,†], Yang Jiao(焦阳)[3,4], Guoqiang Li(李国强)[1], Yu Zheng(郑钰)[3], Qihui Fan(樊琪慧)[5], Gao Wang(王高)[1], Jingru Yao(姚静如)[1], Guo Chen(陈果)[1], Silong Lou(娄四龙)[6], and Liyu Liu(刘雳宇)[1,‡]

[1] *Chongqing Key Laboratory of Soft Condensed Matter Physics and Smart Materials, College of Physics, Chongqing University, Chongqing* 401331, *China*
[2] *Spine Surgery, Beijing Jishuitan Hospital, Beijing* 100035, *China*
[3] *Department of Physics, Arizona State University, Tempe, Arizona* 85287, *USA*
[4] *Materials Science and Engineering, Arizona State University, Tempe, Arizona* 85287, *USA*
[5] *Beijing National Laboratory for Condensed Matter Physics and CAS Key Laboratory of Soft Matter Physics, Institute of Physics, Chinese Academy of Sciences (CAS), Beijing* 100190, *China*
[6] *Department of Neurosurgery, Chongqing University Cancer Hospital, Chongqing* 400030, *China*

(Received 1 June 2021; revised manuscript received 27 June 2021; accepted manuscript online 7 July 2021)

Cell migration in anisotropic microenvironment plays an important role in the development of normal tissues and organs as well as neoplasm progression, *e.g.*, osteogenic differentiation of embryonic stem cells was facilitated on stiffer substrates, indicating that the mechanical signals greatly affect both early and terminal differentiation of embryonic stem cells. However, the effect of anisotropy on cell migration dynamics, in particular, in terms of acceleration profiles which is important for recognizing dynamics modes of cell migration and analyzing the regulation mechanisms of microenvironment in mechanical signal transmission, has not been systematically investigated. In this work, we firstly rigorously investigate and quantify the differences between persistent random walk and anisotropic persistent random walk models based on the analysis of cell migration trajectories and velocity auto-covariance function, both qualitatively and quantitatively. Secondly, we introduce the concepts of positive and negative anisotropy based on the motility parameters to study the effect of anisotropy on acceleration profiles, especially the nonlinear decrease and non-monotonic behaviors. We particularly elaborate and discuss the mechanisms, and physical insights of non-monotonic behaviors in the case of positive anisotropy, focusing on the force exerted on migrating cells. Finally, we analyze two types of *in vitro* cell migration experiments and verify the universality of nonlinear decrease and the consistence of non-monotonic behaviors with numerical results. We conclude that the anisotropy of microenvironment is the cause of the non-monotonic and nonlinear dynamics, and the anisotropic persistent random walk can be as a suitable tool to analyze *in vitro* cell migration with different combinations of motility parameters. Our analysis provides new insights into the dynamics of cell migration in complex microenvironment, which also has implications in tissue engineering and cancer research.

Keywords: cell migration, nonlinear behavior, motility parameter, acceleration profile, anisotropic microenvironment

PACS: 05.10.Gg, 05.40.–a, 05.40.Fb **DOI:** 10.1088/1674-1056/ac11d5

1. Introduction

Cell migration[1,2] is a basic process, which is essential for the normal development of tissues and organs.[3] In particular, a wide range of physiological and pathological processes are involved in cell migration, such as immunological responses,[4] wound healing,[5–7] embryogenesis,[8–11] nervous development.[9,10] However, governed rigorously by complex intra-cellular signaling pathways (ICSP)[12–16] and the extra-cellular matrix (ECM),[2,17–21,23,24] the ill-regulated cell migration leads to many human diseases,[25] among which cancer[26] is the most representative.

As a ubiquitous phenomenon in biology,[1,2] cell migration has been one of the research hotspots, which attracts a lot of attention from mathematicians, physicists and biologists in the past several decades. Initially, cell migration is only viewed as random walk,[27] which is also referred to as Brownian motion.[28,29] For example, the motility of bacteria and eukaryotic cells in the absence of symmetry-breaking gradients.[30,31] Based on Brownian motion, researchers proposed a persistent random walk model (PRW),[32–35] which is highly effective to characterize isotropic cell movement in two-dimensional (2D) ECM. The PRW model obeys the following Langevin equation:[29,36,37]

$$\frac{\mathrm{d}\boldsymbol{v}}{\mathrm{d}t} = -\frac{1}{P}\boldsymbol{v} + \frac{S}{\sqrt{P}}\cdot\tilde{W}, \tag{1}$$

where $\tilde{W} \sim N(0,1)$ is the normalized "white noise" , $\boldsymbol{v}$ is the

*Project supported by the National Natural Science Foundation of China (Grant Nos. 11974066, 11674043, 11675134, and 11874310), the Natural Science Foundation of Chongqing, China (Grant Nos. cstc2019jcyj-msxmX0477 and cstc2018jcyjA3679), and the Capital Health Development Research Project, China (Grant No. 2020-2-2072).

†These authors contributed equally to this work.
‡Corresponding author. E-mail: lyliu@cqu.edu.cn

migration velocity vector, P is the persistence time, and S is the migration speed of the Ornstein–Uhlenbeck (OU) process.[28] Especially, to study the phenomenon that three-dimensional (3D) cell migration does not follow a random walk, a persistent random walk incorporated with cell heterogeneity and local anisotropy has been proposed, *i.e.*, anisotropic persistent random walk (APRW).

In recent years, micropatterning techniques have been greatly developed, which make it possible to confine cells to a patterned geometry and further study the confined dynamics of cell migration. For example, an elastomeric stamp was used to create islands of defined shape, confining cells in predetermined locations and arrays.[38] By analyzing the switch of Human and bovine capillary endothelial cells from growth to apoptosis on micropatterned substrates, a fundamental mechanism for developmental regulation had been represented to explain the role of local geometric patterns in regulating cell growth and viability.[39] In addition, the specific micropatterns and statistical analysis of cell compartment positions indicate that ECM geometry can determine the orientation of cell polarity and also plays an important role in developmental process.[40] Moreover, other geometries have been manufactured, *e.g.*, one-dimentional tracks,[41,42] microratchets,[43,44] micro-structural channel arrays,[45,46] and two-state micropatterns,[23,47,48] *etc.*, in which cell migration experiments can be performed and useful measures such as cell migration speed and persistence (time) can be extracted to quantify cell motility.[49–51]

Except for the micropatterned geometries, some *in vitro* cell migration experiments have been performed to study the role of ECM in determining the behaviors of cell migration.[52] For example, the persistence-driven durokinesis has been observed, which states that cells behave differently on substrates with different rigidities, *i.e.*, cell migration is more persistent on stiffer substrates.[53] Different from the substrates, another crucial component is collagen fibers in ECM, which also greatly affects the behaviors of cell migration.[54,55,57–59] For example, aligned collagen fibers can guide MAD-MB-231 breast cancer cells to invade into rigid matrigel in a constructed ECM,[60] as well as the invasion of cell into 3D funnel-like matrigel interface in a micro-fabricated biochip.[22]

Although a lot of works including numerical simulations and *in vitro* cell experiments, have been done to study the nature of cell migration in complex ECM,[20] few works are involved in the effects of anisotropy of ECM on cell migration dynamics in term of acceleration profiles. In this work, we introduce the PRW and APRW models to simulate cell migration in anisotropic ECM[61,62] and study the role of anisotropy in regulating cell migration, *e.g.*, nonlinear and non-monotonic dynamics, by numerical simulations and *in vitro* cell experiments. The results illustrate that the anisotropy is universal in complex ECM, which can be incorporated into persistent random walk model to describe *in vitro* migration of Dictyostelium discoideum and MCF-10A mammary epithelial cells on 3D collagen gel, to some extent.

The rest of the paper is organized as follows. In Section 2, we apply both quantitative and qualitative approaches to analyze the differences between cell migrations simulated by PRW and APRW models in numerical simulations, especially the analysis of velocity auto-covariance function. In Section 3, we compute and analyze acceleration profiles, exploring the effects of different combinations of motility parameters on cell dynamics based on phase diagram. We also discuss the mechanisms and physical insights of the non-monotonic behaviors, combining with the force exerted on migrating cells. In Section 4, we perform *in vitro* cell migration experiments, and verify universality of nonlinear dynamics and the consistence of non-monotonic behaviors with the results from numerical simulations by fitted motility parameters. Conclusions and discussion are given in Section 5.

2. Two dynamics models describing cell migration

In this section, we aim to introduce two dynamics models describing cell migration in anisotropic ECM. One is the persistent random walk model (PRW), and another is the anisotropic persistent random walk model (APRW). After applying these two models to generate cell migration trajectories in the x–y plane, we initially investigate the differences of cell migration properties due to the differences of ECM.

2.1. Isotropic persistent random walk model

In the past several decades, many of physical models have been developed by researchers to characterize cell migration in certain circumstances. Especially, the inspired PRW model plays an important role and is governed by Eq. (1) in the form of velocity components, as follows:

$$\frac{\mathrm{d}v_x}{\mathrm{d}t} = -\frac{1}{P_x}v_x + \frac{S_x}{\sqrt{P_x}}\cdot\tilde{W}, \tag{2}$$

$$\frac{\mathrm{d}v_y}{\mathrm{d}t} = -\frac{1}{P_y}v_y + \frac{S_y}{\sqrt{P_y}}\cdot\tilde{W}, \tag{3}$$

where P_x, P_y, S_x, and S_y are persistence times and migration speeds, respectively on the x and y axes, all of them are used to quantify cell migration capability. The displacements during cell migration in each time step of Δt are defined as

$$\Delta x(t,\Delta t) = \alpha_x\cdot\Delta x(t-\Delta t,\Delta t) + F_x\cdot\tilde{W}, \tag{4}$$

$$\Delta y(t,\Delta t) = \alpha_y\cdot\Delta y(t-\Delta t,\Delta t) + F_y\cdot\tilde{W}, \tag{5}$$

where Δx and Δy are the displacements of cell location on the x and y axes, and the terms α_x, α_y, F_x, and F_y are memory factors and noise amplitudes, respectively, they are given by

$$\alpha_x = 1-\frac{\Delta t}{P_x},\quad \alpha_y = 1-\frac{\Delta t}{P_y}, \tag{6}$$

$$F_x = \sqrt{\frac{S_x^2 \Delta t^3}{P_x}}, \quad F_y = \sqrt{\frac{S_y^2 \Delta t^3}{P_y}}. \tag{7}$$

The PRW model above [*cf*. Eqs. (2)–(7)] has been widely used to describe the isotropic cell movement in 2D ECM, which denotes that the abilities of cells to move are the same for all directions, there is no preferential direction. Note that the PRW model exhibits a significant characteristic that the velocity auto-correlation function (VACF)[21,63] has the following form:

$$\langle \mathrm{VACF}(\tau) \rangle = \frac{nD}{P} \mathrm{e}^{-\tau P}, \tag{8}$$

where n is the dimension of ECM in which cell migrates, which can be set as 1, 2 or 3. τ is the time lag between any two frames of cell trajectory. D is the diffusion coefficient, which is related to persistence time P and migration speed S, as demonstrated in Ref. [61]. The above VACF indicates that the cell's memory of past velocities satisfies a single-exponential decay. When taking a limit of time lag τ (*e.g.*, infinite), cells can barely remember past velocities, which means that cell migration behaves like the random walk.

After integrating the velocity auto-covariance function twice, we can gain an expression for the mean-square displacement (MSD),[64] as follows:

$$\mathrm{MSD}(\tau) = nS^2P^2 \left(\mathrm{e}^{-\tau/P} + \frac{\tau}{P} - 1 \right), \tag{9}$$

where n, S, and P are the same as those in Eqs. (1) and (8).

2.2. Anisotropic persistent random walk model

Unfortunately, although the PRW model exhibits good performance in describing cell migration in isotropic ECM, it is not appropriate to characterize cell migration in 3D ECM. Differing from 2D cell migration, the 3D cell migration displays high anisotropy, which is mainly caused by the effective substrate stiffness and the physical properties of 3D ECM, *e.g.*, collagen fibers and pore size. The former indicates that cell imaging direction relative to substrate plane will lead to differently persistent migration trajectories, *i.e.* the persistence reaches maximal value when the direction is perpendicular to the plane, while the latter will affect the local properties of trajectory, producing the time-varying characteristics different from the 2D migration. In order to address inappropriateness, Wu *et al*. considered the anisotropy of 3D ECM and proposed the anisotropic persistent random walk model (APRW), see details in Ref. [63]. In numerical simulations, we make motility parameters (P_x and S_x) on the x axis differ from the counterparts (P_y and S_y) on the y axis, corresponding to anisotropic migration.

To explore mechanisms of cell migration in anisotropic ECM, we present comparisons of results obtained from PRW and APRW models, as shown in Fig. 1. Firstly, we simulate cell migration in x–y plane by using the two models above, in which the sampling time is 1 min. Note that we do not consider the effect of localization error (σ_{pos}), because the localization error does not affect the nature of cell migration. Obviously, the migration trajectories [*cf*. Figs. 1(a) and 1(d)] display qualitatively differences, *i.e.*, the trajectory simulated by APRW covers a greater territory in x axis than that in y axis, while the trajectory simulated by PRW almost covers the same territories for x and y axes, according to the scales of axis. In other words, the trajectory simulated by APRW has a preferable direction, which is a direct proof of anisotropy, differing from the isotropic case (PRW).

Furthermore, we compute instantaneous velocity components v_x and v_y by applying the formula $\boldsymbol{v} = \mathrm{d}\boldsymbol{r}/\mathrm{d}t$ (averaged distance every 1 min). The resulting velocity components are exhibited by histograms, as indicated in Figs. 1(b) and 1(e). Clearly, the distribution of v_x [upper panel in Fig. 1(b)] is nearly same as that of v_y [lower panel in Fig. 1(b)], both of them can be fitted by normal Gaussian distributions (see the black lines). The red arrows mark the points of 0 μm/min, corresponding to the peaks of these distributions, which indicate these distributions are symmetry and possess the same probabilities for cell to move forward and backward. The analysis of velocity illustrates that cell migration simulated by PRW is consistent with the OU process, to some extent. Similarly, the counterparts [*cf*. Fig. 1(e)] calculated from APRW also satisfy normal Gaussian distributions with mean values of 0 μm/min, but with a larger difference on the values of variance, which is the consequence of the anisotropic motility parameters in APRW model. Thus, the cell migration in x or y axis meets the OU process, and can be described by different PRW models.

For gaining more insights into the effect of anisotropy on cell migration, we introduce an approach to compute velocity auto-covariance function (VAC),[65] based on velocity components, see details in Figs. 1(c) and 1(f). The black points represent the values of VAC, and the colored dotted lines are auxiliary in log–lin axis, indicating exponential decays in lin–lin axis. Interestingly, we discover an obvious difference in VAC profiles, *i.e.*, the VAC profile follows a single-exponential decay (linearity in log–lin axis) for isotropic case [red dashed line in Fig. 1(c)], while a double-exponential decay (nonlinearity in log–lin axis) for anisotropic case [red and blue dashed lines in Fig. 1(f)]. There is no doubt that the nonlinear behavior contains two migration modes: one is quantified by parameters P_x and S_x, while another is quantified by P_y and S_y, which are consistent with the results obtained from Fig. 1(e), *i.e.*, cell migration in x or y axis satisfies PRW model with different motility parameters. Further, one has access to more insights into the double-exponential behavior by referring to Ref. [61].

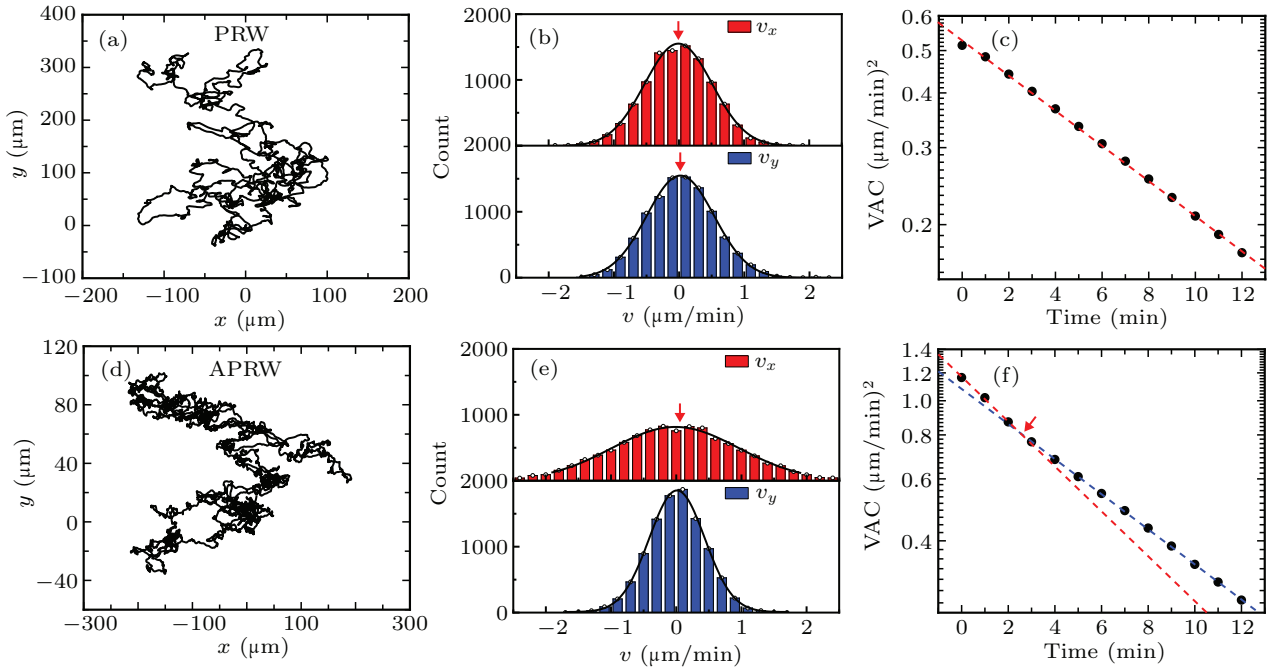

Fig. 1. Comparisons of cell migration simulated by PRW and APRW models. (a) Trajectory starting at the origin (0, 0) in x–y plane and sampled with time interval $\Delta t = 1$ min. The number of recorded frames is $N + 1 = 10001$ (black line). The migration trajectory is simulated by PRW model with a set of parameters ($P_x = P_y = 10$ min, $S_x = S_y = 0.5$ μm/min). (b) Distributions of velocity components (red for v_x and blue for v_y). The migration velocity can be computed from formula $\boldsymbol{v} = \mathrm{d}\boldsymbol{r}/\mathrm{d}t$. (c) Velocity auto-covariance function (black points) based on PRW model. (d)–(f) The captions are corresponding to panels (a)–(c), but the migration trajectory in panel (d) is simulated by APRW model with a set of parameters ($P_x = 10$ min, $P_y = 1$ min, $S_x = 1.0$ μm/min, $S_y = 0.5$ μm/min). The colored dashed lines are auxiliary, and each color corresponds to a single-exponential decay.

3. Anisotropy of ECM triggers the nonlinear cell dynamics

To investigate the effect of anisotropy on cell migration, we apply formula $\boldsymbol{a} = \mathrm{d}\boldsymbol{v}/\mathrm{d}t$ to compute the acceleration in different manners, as a function of instantaneous velocity. By analyzing the acceleration profiles, we investigate the role of anisotropy in regulating cell migration dynamics in anisotropic ECM.

3.1. Linear cell dynamics

In Fig. 1, we analyze the cell migration simulated by PRW and APRW models, and find the latter is consistent with OU process to some extent, and anisotropy does affect cell behavior. To explore the mystery of cell dynamics and verify the effect in other aspects, we firstly compute acceleration components a_x and a_y based on the isotropic trajectory in Fig. 1(a). The scatter diagrams [cf. Fig. 2(a)] of acceleration components a_x and a_y are plotted against the corresponding velocity components v_x and v_y, respectively. The corresponding bin-averaged acceleration components in Fig. 2(b) show that they decrease linearly as the velocity components increase. Further, the statistical histograms of the acceleration components also manifest that both of the acceleration components are fitted well by the Gaussian distributions with mean values smaller than 0 μm/min^2, as shown in Fig. 2(c). With the same meanings, the red arrows mark the points of 0 μm/min^2, and it is obvious that the peaks of the Gaussian distributions are slightly smaller than 0 μm/min^2, corresponding to the decreasing negative accelerations in Fig. 2(b).

Next, we explore the relationship between acceleration components parallel and orthogonal to velocity, respectively. The acceleration components a_p and a_o scattered in Fig. 2(d) are generated as follows: (i) picking any two successive velocities computed from cell migration trajectory, (ii) computing the components of second velocity relative to the first velocity, (iii) calculating acceleration components parallel and orthogonal to the first velocity, and (iv) plotting acceleration components scatters against migration velocity.

The bin-averaged acceleration components a_p and a_o in Fig. 2(e) clearly show that they are subject to different trends as the velocity increases. The bin-averaged a_o hardly varies with the velocity and have a mean value of 0 μm/min^2, while the bin-averaged a_p linearly decreases with the increase of velocity. Note that the fluctuation of bin-averaged acceleration components corresponding to high velocity, *e.g.*, the interval 1.25 μm/min ∼ 2.0 μm/min in Fig. 2(e), is due to the small sample size [see the sparse points in Figs. 2(a) and 2(d)]. This linear decreasing behavior [cf. Fig. 2(e)] is a characteristic of OU model, as indicated in Eq. (10). It is clear that cell acceleration is a random vector for any time t, because of the presence of Gaussian white noise. What is more, the random vector has an expectation value, as follows:

$$\langle \boldsymbol{a}_v \rangle_{\boldsymbol{v}} = \left\langle \frac{\mathrm{d}\boldsymbol{v}}{\mathrm{d}t} \right\rangle_{\boldsymbol{v}} = -\frac{1}{P}\boldsymbol{v}, \tag{10}$$

which characterizes the linear decreasing behavior in Fig. 2(e) and its component forms also describe the same behaviors in Fig. 2(b). The term $-1/P$ is the slope of expectation value, and it determines how fast the acceleration component $a_{\rm p}$ linearly decreases. In Fig. 2(f), the distribution of $a_{\rm p}$ is asymmetric and the mean value of the distribution is smaller than 0 μm/min^2, which differs from that for $a_{\rm o}$, but is the same as those in Fig. 2(c).

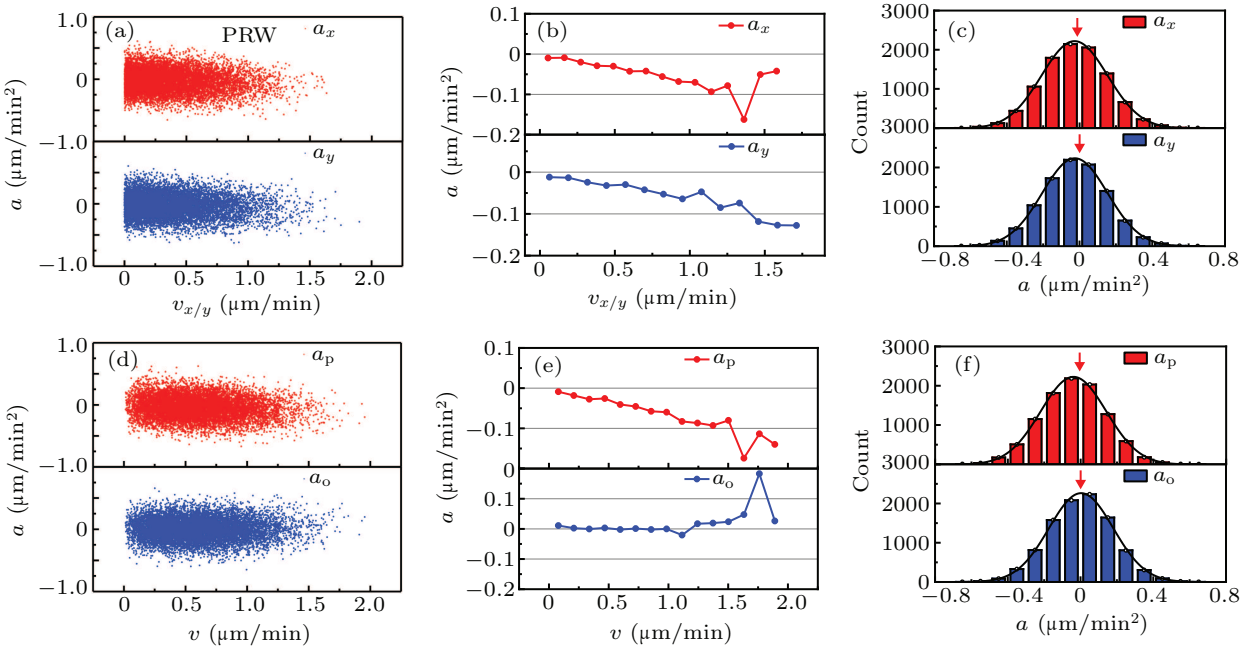

Fig. 2. Linear dynamics of cell migration in isotropic ECM. (a) The computed acceleration components parallel to x axis (red for a_x) and parallel to y axis (blue for a_y), plotted against cell migration velocity components (v_x and v_y). (b) The bin-averaged acceleration components as functions of migration velocity components (v_x and v_y). (c) Distributions of acceleration components a_x and a_y. (d) The computed acceleration components parallel (red for $a_{\rm p}$) and orthogonal (blue for $a_{\rm o}$) to the cell migration velocity, plotted against cell migration velocity (v). (e) The bin-averaged acceleration components, as functions of migration velocity. (f) Distributions of acceleration components $a_{\rm p}$ and $a_{\rm o}$.

3.2. Nonlinear cell dynamics

In what follows, we continue to analyze anisotropic cell migration dynamics in the same manner as that applied in isotropic case. Here, the analysis of cell dynamics is based on the anisotropic trajectory shown in Fig. 1(d), and the resulting calculations are displayed in Fig. 3. Note that the distributions of acceleration components a_x and a_y still satisfy Gaussian distributions with mean values smaller than 0 μm/min^2, despite the large difference between these two scatter diagrams in high velocity domain.

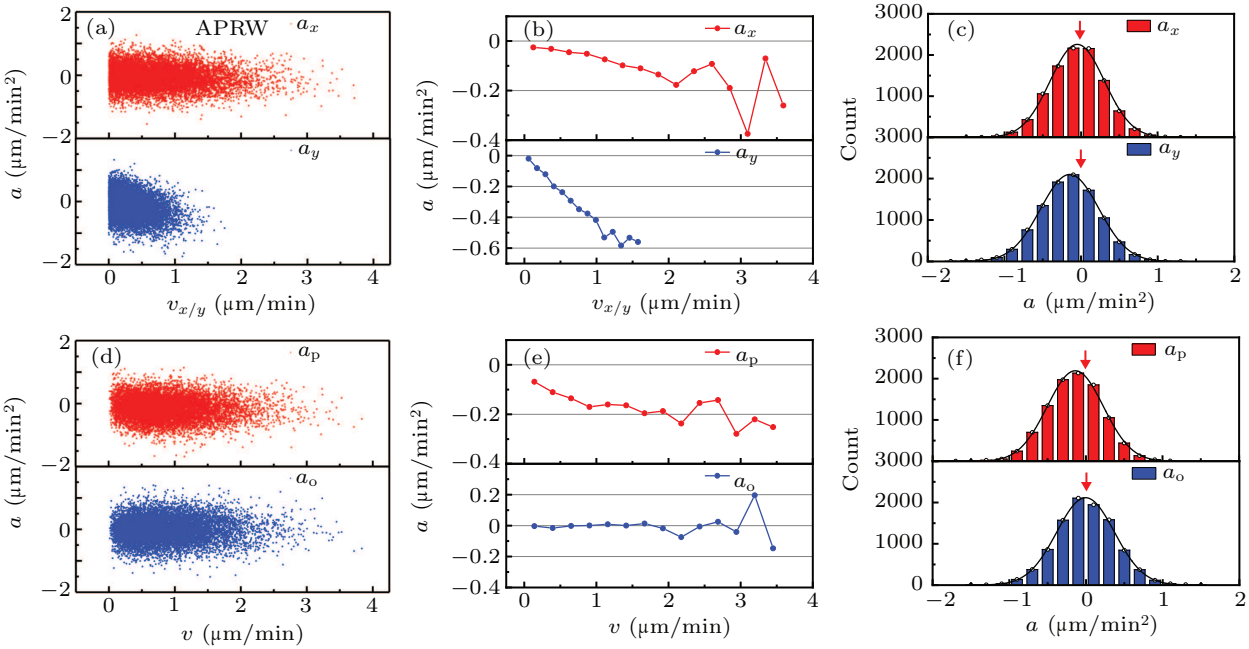

Fig. 3. Nonlinear dynamics of cell migration in anisotropic ECM. The captions are identical with those for Fig. 2, but the results corresponds to cell migration trajectories simulated by ARRW model.

There is an interesting phenomenon that the bin-averaged acceleration component a_{p} decrease nonlinearly over the velocity in Fig. 3(e), which differs from the linear decrease in Fig. 2(e). Thus, we argue that the anisotropy of ECM is the cause of nonlinearity in acceleration component a_{p}. Further, it is attractive that both the one-dimensional (1D) migrations on the x and y directions are consistent with OU process, but the resultant motion of these two 1D migrations exhibits a novel property, which is different from that predicted by OU process.

In contrast to the expectation value described by Eq. (10) for the PRW model, we deduce the similar relationship on the x and y axes for the APRW model, which is defined as follows:

$$\langle \boldsymbol{a}_v \rangle_{\boldsymbol{v}} = \left\langle \frac{\mathrm{d}\boldsymbol{v}}{\mathrm{d}t} \right\rangle_{\boldsymbol{v}} = -\frac{1}{P_x}\boldsymbol{v}_x - \frac{1}{P_y}\boldsymbol{v}_y. \tag{11}$$

This expression indicates that the acceleration component in individual x or y direction follows a linear decrease, but a nonlinear decrease for the resultant motion. Here, the nonlinearity is mainly the consequence of different values of P_x and P_y.

3.3. The effect of anisotropy on cell dynamics

In this section, we perform several control simulations about cell migration to study how the acceleration component a_{p} changes for different combinations of parameter values. To better quantify the anisotropy of ECM, we introduce a quantity, *i.e.*, anisotropy index Φ,[61] which can be written as

$$\Phi = \max\left\{\frac{P_x \cdot S_x^2}{P_y \cdot S_y^2}, \frac{P_y \cdot S_y^2}{P_x \cdot S_x^2}\right\}. \tag{12}$$

Furthermore, we also define anisotropy index of persistence time and migration speed, separately. They are given as follows:

$$\Phi_{\mathrm{P}} = \max\left\{\frac{P_x}{P_y}, \frac{P_y}{P_x}\right\}, \tag{13}$$

$$\Phi_{\mathrm{S}} = \max\left\{\frac{S_x^2}{S_y^2}, \frac{S_y^2}{S_x^2}\right\}. \tag{14}$$

Clearly, all the indexes are dimensionless values and greater than unity. Due to the inspiration of anisotropy index, we define two concepts based on the motility parameters, *i.e.*, positive anisotropy (PA) and negative anisotropy (NA). The detail definition as follows: if the persistence time and migration speed in one direction (such as x axis), are greater than the values in another direction (such as y axis), respectively, then we refer the case to as positive anisotropy, otherwise it is negative anisotropy.

In Fig. 4, we aim to explore how the acceleration component a_{p} changes in the cases of positive anisotropy and negative anisotropy. Firstly, we investigate the effect of Φ_{P} when $S_x = S_y$. As the increase of Φ_{P} from 2.5 to 20.0, the a_{p} profiles become more nonlinear, corresponding to the tendency of downward concave, as shown in Fig. 4(a). Based on the values of motility parameters in Fig. 4(a), we just modify the values of migration speed, and make S_x greater than S_y (PA). The a_{p} profiles become more interesting [*cf.* Fig. 4(b)] because of a non-monotonic behavior that the values of a_{p} increase as the increase of velocity, in the context of downward concave. See Fig. 6 for more details about this non-monotonic behavior. Similarly, we make S_x less than S_y (NA), and keep other parameters constant [*cf.* Fig. 4(c)]. The a_{p} profiles change the ways they decrease, and produce the tendency of upward convex.

In a similar manner, we analyze the effect of Φ_{S} on the ways a_{p} profiles decrease. In Fig. 4(d), we make $P_x = P_y$, and increase the values of Φ_{S} from 1.6 to 25.0. The a_{p} profiles clearly show that the increase of Φ_{S} does not change the linearity of profiles, but the scale of profiles. When adjusting the values of persistence time and make P_x greater than P_y (PA), the a_{p} profile becomes nonlinear, forming the tendency of downward concave. As a whole, all a_{p} profiles in Fig. 4(e) almost have the same tendencies, but with different scales. It means that the Φ_{S} only changes the scale of profile, not the way a_{p} profile decreases. For the case of P_x less than P_y (NA) in Fig. 4(f), all a_{p} profiles almost obey the tendency of upward convex.

To vividly exhibit the transition of a_{p} profiles induced by anisotropic motility parameters, we calculate the phase diagram of a_{p} behaviors following the procedures:

(i) referring the line segments formed by points in a_{p} profile to as vectors;

(ii) computing the angle between any two vectors;

(iii) multiplying $+1$ and the angle when the second vector is biased to the right relative to the first vector (*i.e.*, tendency of upward convex), otherwise multiplying -1 and the angle (*i.e.*, tendency of downward concave);

(iv) averaging the angles and plotting the phase diagram, as seen in Fig. 5.

Obviously, there are four sections in this figure, *i.e.*, left-top, left-bottom, right-top, and right-bottom. Left-top and right-bottom are almost represented by positive angles (red), which denotes that the corresponding a_{p} profiles possess the tendencies of upward convex. Meanwhile, the left-bottom and right-top are almost represented by negative angles (blue), indicating a_{p} profiles possess the tendencies of downward concave. In addition, the averaged angles for $P_x/P_y = 1$ slightly deviate from the theoretical value 0, which is the consequence of limited data.

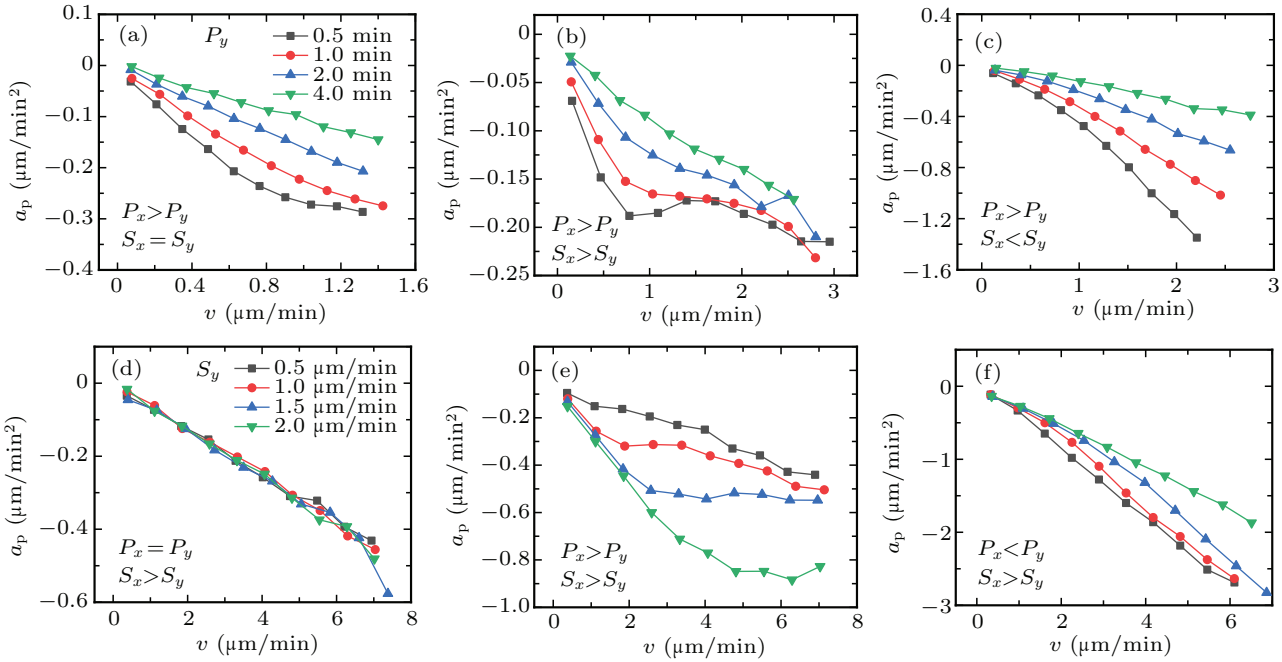

Fig. 4. The effects of anisotropy on cell migration dynamics in complex ECM. (a) The effects of anisotropy of persistence time P on cell migration dynamics. Let $S_x = S_y = 0.5$ μm/min, and $P_x = 10$ min, increasing the value of P_y from 0.5 min to 4.0 min. (b) The effects of anisotropy of persistence time P on cell migration dynamics in the case of positive anisotropy. The values of P_x and P_y are the same as those in panel (a), but $S_x = 1.0$ μm/min and $S_y = 0.5$ μm/min. (c) The effects of anisotropy of persistence time P on cell migration dynamics in the case of negative anisotropy. The values of P_x and P_y are the same as those in panel (a), but $S_x = 0.5$ μm/min and $S_y = 1.0$ μm/min. (d) The effects of anisotropy of migration speed S on cell migration dynamics. Let $P_x = P_y = 10.0$ min, and $S_x = 2.5$ μm/min, increasing the value of S_y from 0.5 μm/min to 2.0 μm/min. (e) The effects of anisotropy of migration speed S on cell migration dynamics in the case of positive anisotropy. The values of S_x and S_y are the same as those in panel (d), but $P_x = 10.0$ min and $P_y = 1.0$ min. (f) The effects of anisotropy of migration speed S on cell migration dynamics in the case of negative anisotropy. The values of S_x and S_y are the same as those in panel (d), but $P_x = 1.0$ min and $P_y = 10.0$ min.

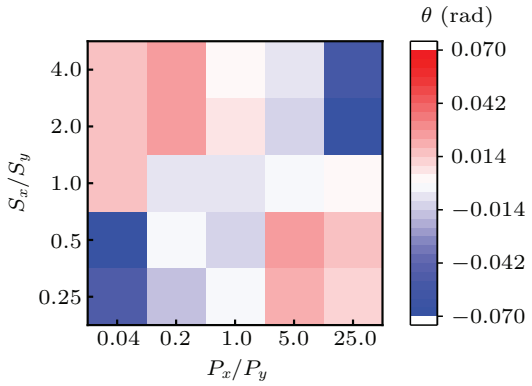

Fig. 5. Phase diagram of the nonlinear behavior in complex ECM. The horizontal axis represents P_x/P_y, while the vertical axis represents S_x/S_y. The color bar denotes the averaged angle θ corresponding to the nonlinearity of a_p profile. $P_x/P_y = 1$ corresponds to the parameters $P_x = P_y = 10$ min, while $S_x/S_y = 1$ corresponds to the parameters $S_x = S_y = 2$ μm/min.

Thus, we can conclude that firstly, regardless of the values of migration speed, the anisotropy of persistence time leads to the nonlinear a_p profiles, see Fig. 4 [except for panel (d)]. Secondly, the positive anisotropy produces the tendency of downward concave in the case where Φ_P is small, while the negative anisotropy produces the tendency of upward convex, see Figs. 4(b)–4(c) and 4(e)–4(f). Especially the non-monotonic behavior occurs as the increase of Φ_P, in the case of positive anisotropy [see gray and red lines in Fig. 4(b)]. Then, increasing the anisotropy of persistence time facilitates a_p profile to be more nonlinear, in the cases of positive and negative anisotropy, see Figs. 4(b) and 4(c). Finally, increasing the anisotropy of migration speed only changes the scale of a_p profile, not the way it decreases, see Figs. 4(e) and 4(f). The phase diagram in Fig. 5 also validates that the anisotropic motility parameters (or ECM) will affect the nonlinear dynamics of cell migration.

3.4. Non-monotonic cell dynamics in anisotropic ECM

In Fig. 4(b), we discover that a non-monotonic behavior occurs in a_p profile in the case of positive anisotropy, especially for a large anisotropy of persistence time (Φ_P). In what follows, we explicitly regulate the Φ_P to study how the non-monotonic behavior changes in the case of positive anisotropy.

To capture the major changes of a_p profile, we mark two representative points in a_p profile, which are concave and convex, respectively. One is viewed as valley, while another is viewed as peak, as indicated in Fig. 6(a). We increase the values of P_y from 0.15 min to 2.15 min, for a given set of parameters ($P_x = 20$ min, $S_x = 1.0$ μm/min, and $S_y = 0.5$ μm/min). Note that the Φ_P ranges from 133.3 to 9.3 when $\Phi_S = 2$. As the value of P_y increases, the abscissa (blue scatters) of the valley increases stepwise. The three speed domains correspond to 0.15 min $\sim$ 0.5 min, 0.5 min $\sim$ 1.25 min, and 1.25 min $\sim$ 2.15 min, respectively, as indicated by the black ladder in Fig. 6(b). However, the abscissa (red scatters) of the peak undergoes two steps, first increases and then decreases. In contrast to the way the abscissa changes, both the ordinates of the valley and the peak experience a "roller coaster", *i.e.*,

first decrease, then increase, and finally reach the same value, as demonstrated in Fig. 6(c). The roller coaster implies two events, one is the appearance of non-monotonic behavior, and another is the disappearance of non-monotonic behavior.

To gain more insights into the relationship between the anisotropy of persistence time and the non-monotonic behavior, we study the rectangle with the valley and peak as vertexes, and its orthogonal sides are parallel to the x and y axes, respectively, see the dotted lines in Fig. 6(a). Figures 6(d)–6(f) manifest that the distances between valley and peak on the x and y directions and the corresponding area obey the tendency, *i.e.*, increase first and then decrease. Thus, we obtain an overall picture about the changes of $a_{\rm p}$ profile when changing the anisotropy of persistence time.

The non-monotonic behavior signifies that the $a_{\rm p}$ profile is not a monotonically decreasing function of velocity, but contains an interval where the values of $a_{\rm p}$ increase. Here, we argue that, the increasing part clearly hints that the net force on the cell gradually decreases, as the velocity increases. Thus, we can deduce the force exerted on cell during migration, which is given as

$$F^* = F_{\rm r} - F_{\rm d}, \tag{15}$$

where $F_{\rm d}$ is the force that drives the cell forward, $F_{\rm r}$ is the force that impedes cell migration, and F^* is the net force. The above equation (15) is analogous to Eq. (1), the Gaussian white noise corresponds to $F_{\rm d}$, while $-\boldsymbol{v}/P$ corresponds to $F_{\rm r}$. Considering that the Gaussian white noise can be viewed as constant in the regime of long time scale, thus the term $F_{\rm r}$ will lead to the changes in $a_{\rm p}$ profile, especially non-monotonic behavior. The behavior indicates that the greater the velocity of one cell, the less the resistance it will experience, which does not conform to the widely accepted law, *i.e.*, the greater the velocity of a body, the greater the resistance it will experience.

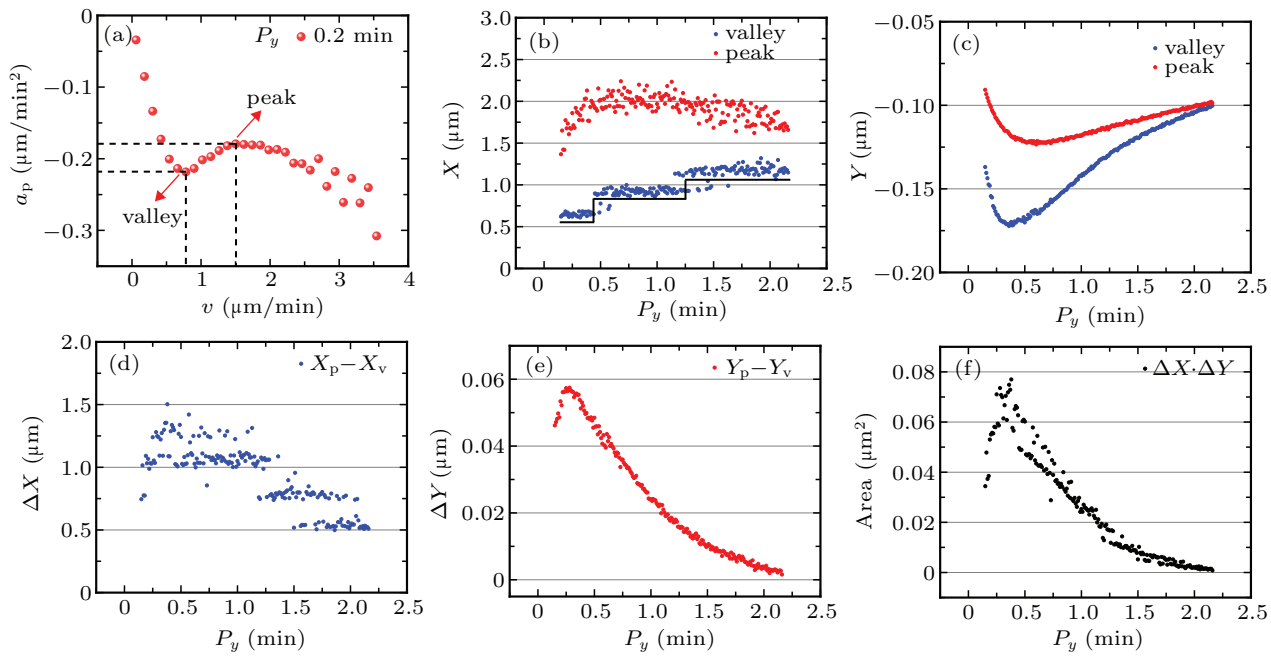

Fig. 6. Positive anisotropy leads to non-monotonic cell dynamics. (a) A recessed part of the acceleration component ($a_{\rm p}$) parallel to cell's velocity plotted against migration velocity (red point), for a given set of parameters ($P_x = 10$ min, $P_y = 0.2$ min, $S_x = 0.8$ μm/min, and $S_y = 0.6$ μm/min). (b) The abscissa of valley (blue) and peak (red) of $a_{\rm p}$ profile as a function of P_y. The value of P_y ranges from 0.15 min to 2.15 min for a given set of parameters ($P_x = 20$ min, $S_x = 1.0$ μm/min, and $S_y = 0.5$ μm/min). (c) The ordinate of valley (blue) and peak (red) of $a_{\rm p}$ profile as a function of P_y. (d) The difference (blue) between the abscissa of valley and peak of $a_{\rm p}$ as a function of P_y. (e) The difference (red) between the ordinate of valley and peak of $a_{\rm p}$ profile as a function of P_y. (f) The area formed by peak and valley as a function of P_y.

4. Nonlinear dynamics for *in vitro* cell migration

We have analyzed the effect of anisotropy on cell migration dynamics based on numerical simulations, *i.e.*, discussing the changes in acceleration profiles, and find there is a non-monotonic behavior that acceleration component $a_{\rm p}$ gradually increases in a certain velocity interval. In this section, we analyze the *in vitro* cell migration experiments and verify the universality of nonlinear and non-monotonic behaviors and the consistence with the results predicted by APRW model by fitted motility parameters.

4.1. The non-monotonic behavior for Dictyostelium discoideum

In this part, we follow the procedure used above to analyze *in vitro* experimental data, which are obtained from Ref. [15]. Note that the authors analyzed the role of Arpin protein in regulating the directionality of cell migration, we only choose the migration data for wild-type (WT) Dictyostelium discoideum. The corresponding results are shown in Fig. 7.

We firstly compute the acceleration components $a_{\rm p}$ and $a_{\rm o}$, which are shown in Figs. 7(a) and 7(c). On the basis of the

acceleration scatter diagrams, we bin-averaged the a_p and a_o, respectively, as indicated in Figs. 7(b) and 7(d). The a_p profile also exhibits the non-monotonic behavior, *i.e.*, there is an non-monotonic part where the a_p profile gradually increases as the velocity increases. The non-monotonic behavior is almost identical with that shown in Fig. 6(a). Especially, the a_o profile fluctuates around at 0 μm/min^2, which is close to the results shown in Figs. 2 and 3.

In addition, we also compute VAC and MSD, as indicated in Figs. 7(e) and 7(f). The VAC obeys a nonlinear exponential decay in log–lin axis, which mainly contains two migration modes, one is marked by red dotted line and another is marked by blue dotted line. Here, the nonlinear VAC is consistent with that in Fig. 1(f). Following the procedure in Ref. [61], we fit the calculated VAC with the superimposed form of theoretical formula defined in Refs. [51,65] and obtain the fitted VAC and the corresponding motility parameters, as seen in Fig. 7(e). The fitted motility parameters are $P_1 = 0.339$ min, $S_1 = 6.245$ μm/min, $P_2 = 0.036$ min, $S_2 = 4.913$ μm/min, respectively, which satisfies the criteria of positive anisotropy because of $P_1 > P_2$, $S_1 > S_2$. In addition, the MSD in Fig. 7(f) lies at the interval ranging from the red line with a slope 2 to the blue line with a slope 1, which illustrates that the migration of Dictyostelium discoideum can be described by persistent walk model, *e.g.*, PRW or APRW model to some extent. The MSD also exhibits distinguishable behaviors at different time scales, *i.e.*, it grows quadratically just like ballistic motion in the regime of short lag-times (< 0.8 min), while grows linearly just like pure Brownian motion in the regime of long lag-times (> 0.8 min), thus there must be a point reflecting the ensemble-average characteristics of cell migration. Moreover, in the regime of short lag-times, the MSD gradually deviates from the ballistic motion, which indicates that cell gradually loses the memory of the past velocities as the lag-time increases.

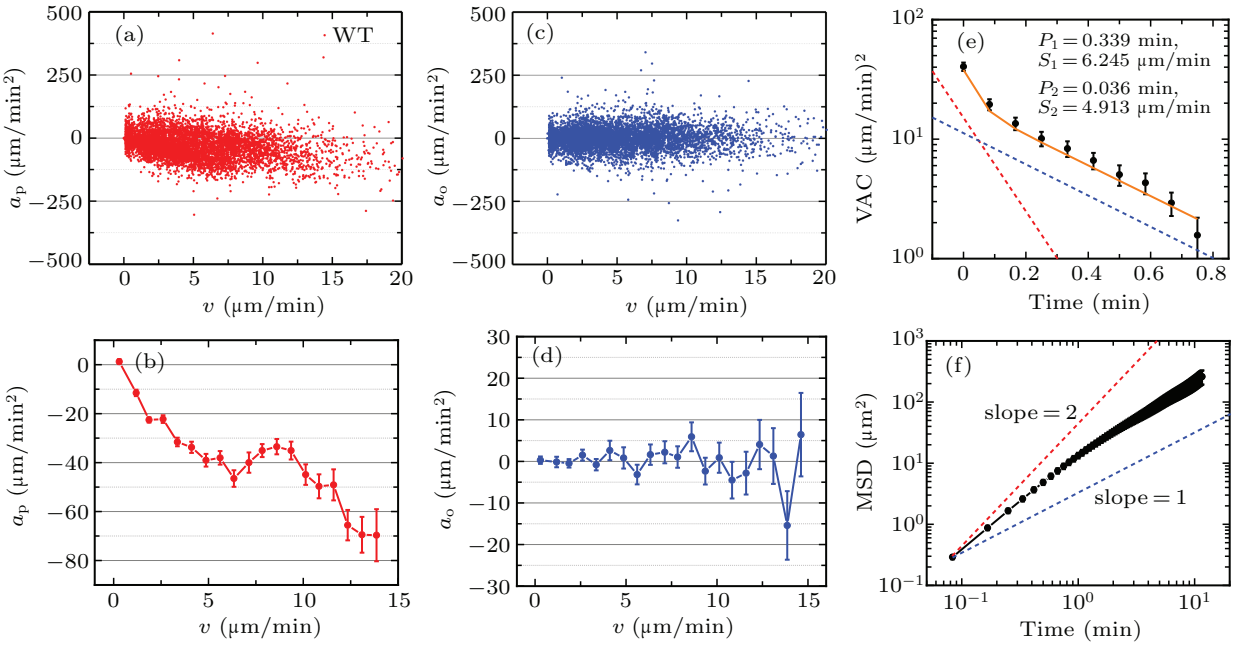

Fig. 7. The non-monotonic migration dynamics for wild-type Dictyostelium discoideum. (a) The computed acceleration components a_p plotted against cell migration velocity. (b) The bin-averaged acceleration component a_p as a function of migration velocity. (c) The computed acceleration components a_o plotted against cell migration velocity. (d) The bin-averaged acceleration component a_o as a function of migration velocity. (e) Velocity auto-covariance function as a function of time. The red and blue dotted lines denote two single-exponential decay functions and the orange line denotes the fitted results. (f) Mean-square displacement as a function of time. The red dotted line corresponds to the ballistics motion with a slope 2, while the blue dotted line corresponds to the Brownian motion with a slope 1. The data are represented by mean ±SE (standard error of the sample mean); the number of cells is 43.

Based on the analysis above, it is reasonable to conclude that: (i) the migration of wild-type Dictyostelium discoideum, at least can be described by APRW model because of the nonlinear VAC and the non-monotonic acceleration a_p; (ii) the non-monotonic behavior in acceleration profile illustrates that motility parameters meet the condition of positive anisotropy and there is a greater difference between two persistence times (high anisotropy); (ii) the fitted motility parameters fitted from VAC do validate the consistence with the results from APRW model.

4.2. The nonlinear behavior for MCF-10A mammary epithelial cells migration on 3D collagen gel

To verify the universality of the nonlinear cell dynamics and the consistence with the numerical results, we analyze the *in vitro* cell migration data, *i.e.*, MCF-10A mammary epithelial cells migration on 3D collagen gel, see more detail experimental procedures in Ref. [50]. We perform the same calculations and obtain the corresponding results in Fig. 8.

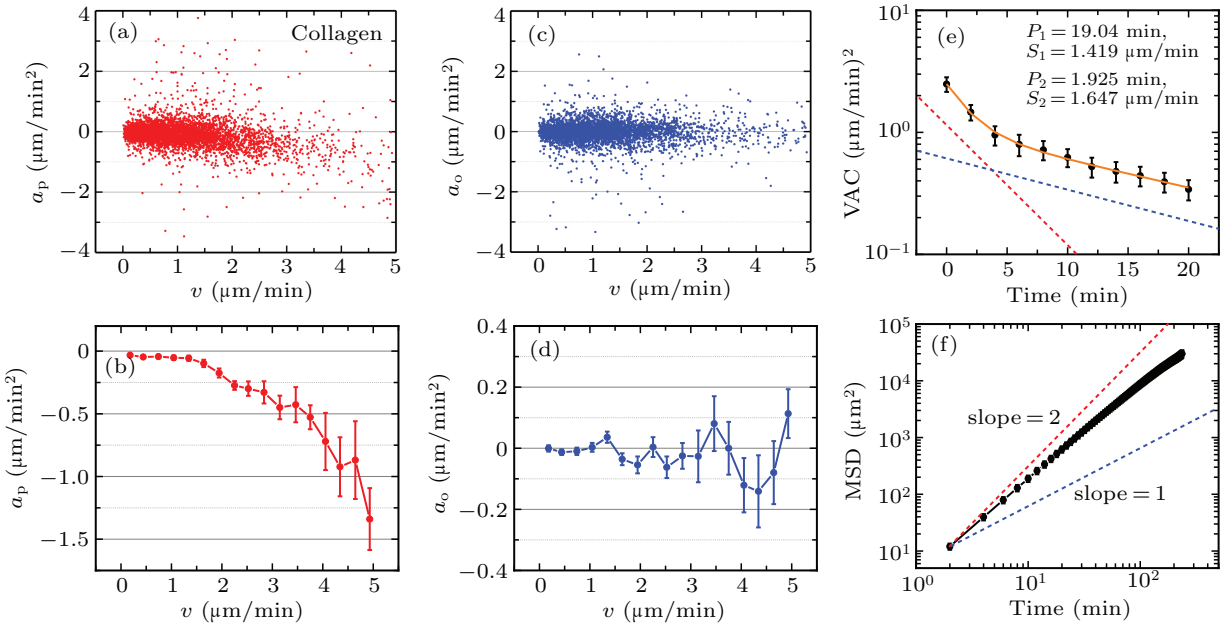

Fig. 8. The nonlinear migration dynamics for MCF-10A mammary epithelial cells migration on 3D collagen gel. The captions are identical with those in Fig. 7. The data are represented by mean ±SE; the number of cells is 42.

When compared with results in Fig. 7, we find the VAC and MSD [*cf*. Figs. 8(e) and 8(f)] obey the same tendencies with those for wild-type Dictyostelium discoideum. The only difference is that the a_p profile shows no non-monotonic behavior, but nonlinear, which is similar with that in Fig. 4(c). Meanwhile, the fitted motility parameters from VAC are $P_1 = 19.04$ min, $S_1 = 1.419$ μm/min, $P_2 = 1.925$ min, $S_2 = 1.647$ μm/min, respectively, which satisfies the criteria of negative anisotropy because of $P_1 > P_2$, $S_1 < S_2$. Thus, we can conclude that (i) the migration of MCF-10A mammary epithelial cells on 3D collagen gel also may be described by APRW model because of the nonlinear VAC and the nonlinear acceleration; (ii) the nonlinear behavior indicates that motility parameters meet the condition of negative anisotropy, which is further validated by the fitted motility parameters.

5. Discussion and conclusion

In this work, we firstly introduce two models, PRW and APRW, to analyze the influence of anisotropy of ECM on cell migration dynamics. Qualitatively, the trajectory pattern simulated by APRW model is more persistent than that by PRW model and the persistence is validated by VAC, *i.e.*, the values of VAC computed from APRW model are greater than those from PRW model for a given time lag τ. What is more, in contrast to the single-exponential decay of VAC computed from PRW model, the VAC computed from APRW model follows a double-exponential decay corresponding to two migration modes. In addition, we find that both distributions of velocity components on the x and y axes obey normal Gaussian distributions with mean values 0 μm/min, which means that the cell migration on the x or y axis follows the OU process, to some extent.

Secondly, we compute the acceleration components, *e.g.*, a_x, a_y, a_p, a_o, and investigate the distributions of different acceleration components. The results indicate both the acceleration components on the x and y axes are linearly decreasing functions of velocity components. This linear decrease exactly verifies the result mentioned above, *i.e.*, the cell migration in x or y axis follows the OU process. The acceleration component parallel to the instantaneous velocity, for PRW and APRW models, reveals different behaviors. The parallel acceleration component a_p is still a linearly decreasing function of velocity for PRW model, but a nonlinearly decreasing function for APRW model. Furthermore, whether or not the acceleration component deceases, is related to the mean value of distribution of acceleration component: if acceleration component is a decreasing function of velocity, then the mean value of distribution is smaller than 0 μm/min^2, otherwise it equals 0 μm/min^2.

Then, to investigate the effects of combinations of motility parameters, we introduce positive and negative anisotropies by setting different parameter values in APRW model, and find that positive anisotropy leads to a downward concave in a_p profile, while negative anisotropy leads to an upward convex based on phase diagram. In particular, the anisotropies of persistence time and migration speed only influence the nonlinearity and scale of a_p profile, respectively. We further discover that the anisotropy of persistence time results in a non-monotonic behavior occurring in a_p profile in the case of positive anisotropy.

Finally, we follow the same procedure to analyze two types of *in vitro* cell migration experiments, *i.e.*, the migration of wild-type Dictyostelium discoideum and MCF-10A mammary epithelial cells migration on 3D collagen gel. The results indicate that the a_{p} profile for Dictyostelium discoideum show non-monotonic behavior and that for MCF-10A cells show nonlinear behavior, which are consistent with the results obtained from APRW model, especially the fitted motility parameters further validate the consistence.

Our work presents the relationship between the anisotropy of ECM and cell migration dynamics in term of acceleration profile, and emphasizes the importance of the anisotropy during cell migration, especially the VAC following a double-exponential decay, the nonlinear decrease and the non-monotonic behavior of a_{p} profile. We conclude that the anisotropy of ECM in which cell migrates is the cause of the non-monotonic and nonlinear dynamics, and the APRW model can be as a suitable tool to analyze *in vitro* cell migration with different combinations of motility parameters. The work provides new insights into the dynamics of cell migration in complex ECM, which also has implications in tissue engineering and cancer research.

References

[1] Berg H C and Dyson F *Phys. Today* **40** 73
[2] Vicente-Manzanares M and Horwitz A R 2011 *Methods in molecular biology* (Clifton, N.J.) **769** 1
[3] Cyster J G 2003 *Immunolog. Rev.* **195** 5
[4] Luster A D, Alon R and von Andrian U H 2005 *Nature Immunology* **6** 1182
[5] Martin P 1997 *Science* **276** 75
[6] Tremel A, Cai A, Tirtaatmadja N, Hughes B D, Stevens G W, Landman K A and O'Connor A J 2009 *Chem. Eng. Sci.* **64** 247
[7] Franz A, Wood W and Martin P 2018 *Developmental Cell* **44** 460
[8] Zalokar M and Erk I 1976 *Journal De Microscopie Et De Biologie Cellulaire* **25** 97
[9] Natarajan D, Marcos-Gutierrez C, Pachnis V and de Graaff E 2002 *Development* **129** 5151
[10] Kulesa P, Ellies D L and Trainor P A 2004 *Developmental Dynamics* **229** 14
[11] Takakura N, Watanabe T, Suenobu S, Yamada Y, Noda T, Ito Y, Satake M and Suda T 2000 *Cell* **102** 199
[12] Ridley A J, Schwartz M A, Burridge K, Firtel R A, Ginsberg M H, Borisy G, Parsons J T and Horwitz A R 2003 *Science* **302** 1704
[13] Sharma G D, He J C and Bazan H E P 2003 *J. Bio. Chem.* **278** 21989
[14] Schaffer A E, Breuss M W, Caglayan A O, Al-Sanaa N, Al-Abdulwahed H Y, Kaymakcalan H, Yilmaz C, Zaki M S, Rosti R O, Copeland B, Baek S T, Musaev D, Scott E C, Ben-Omran T, Karimine-jad A, Kayserili H, Mojahedi F, Kara M, Cai N, Silhavy J L, Elsharif S, Fenercioglu E, Barshop B A, Kara B, Wang R G, Stanley V, James K N, Nachnani R, Kalur A, Megahed H, Incecik F, Danda S, Alanay Y, Faqeih E, Melikishvili G, Mansour L, Miller I, Sukhudyan B, Chelly J, Dobyns W B, Bilguvar K, Abou Jamra R, Gunel M and Gleeson J G 2018 *Nature Genetics* **50** 1093
[15] Dang I, Gorelik R, Sousa-Blin C, Derivery E, Guerin C, Linkner J, Nemethova M, Dumortier J G, Giger F A, Chipysheva T A, Ermilova V D, Vacher S, Campanacci V, Herrada I, Planson A G, Fetics S, Henriot V, David V, Oguievetskaia K, Lakisic G, Pierre F, Steffen A, Boyreau A, Peyrieras N, Rottner K, Zinn-Justin S, Cherfils J, Bieche I, Alexandrova A Y, David N B, Small J V, Faix J, Blanchoin L and Gautreau A 2013 *Nature* **503** 281
[16] Lauffenburger D A and Horwitz A F 1996 *Cell* **84** 359
[17] Bergman A J and Zygourakis K 1999 *Biomaterials* **20** 2235
[18] Lo C M, Wang H B, Dembo M and Wang Y L 2000 *Biophys. J.* **79** 144
[19] Raines E W 2000 *International Journal of Experimental Pathology* **81** 173
[20] Polacheck W J, Zervantonakis I K and Kamm R D 2013 *Cellular and Molecular Life Sciences* **70** 1335
[21] Wu P H, Giri A, Sun S X and Wirtz D 2014 *Proc. Natl. Acad. Sci. USA* **111** 3949
[22] Zhu J, Liang L, Jiao Y, Liu L and Allianc U S-C P S-O 2015 *Plos One* **10** UNSP e0118058
[23] Fink A, Bruckner D B, Schreiber C, Rottgermann P J F, Broedersz C P and Radler J O 2020 *Biophys. J.* **118** 552
[24] Kim J, Zheng Y, Alobaidi A A, Nan H Q, Tian J X, Jiao Y and Sun B 2020 *Biophys. J.* **118** 1177
[25] Hanahan D and Weinberg R A 2011 *Cell* **144** 646
[26] Jemal A, Siegel R, Xu J and Ward E 2010 *Ca-a Cancer Journal for Clinicians* **60** 277
[27] Codling E A, Plank M J and Benhamou S 2008 *Journal of the Royal Society Interface* **5** 813
[28] Uhlenbeck G E and Ornstein L S 1930 *Phys. Rev.* **36** 0823
[29] Lemons D S and Gythiel A 1997 *Am. J. Phys.* **65** 1079
[30] Darnton N C, Turner L, Rojevsky S and Berg H C 2010 *Biophys. J.* **98** 2082
[31] Li L, Norrelykke S F and Cox E C 2008 *Plos One* **3** e2093 11
[32] Wu H, Li B L, Springer T A and Neill W H 2000 *Ecological Modelling* **132** 115
[33] Weiss G H 2002 *Physica a-Statistical Mechanics and Its Applications* **311** Pii s0378-4371(02)00805-1 381
[34] Li L, Cox E C and Flyvbjerg H 2011 *Physical Biology* **8** 046006
[35] Selmeczi D, Mosler S, Hagedorn P H, Larsen N B and Flyvbjerg H 2005 *Biophys. J.* **89** 912
[36] Schienbein M and Gruler H 1993 *Bulletin of Mathematical Biology* **55** 585
[37] Burov S and Barkai E 2008 *Phys. Rev. Lett.* **100** 070601
[38] Singhvi R, Kumar A, Lopez G P, Stephanopoulos G N, Wang D I C, Whitesides G M and Ingber D E 1994 *Science* **264** 696
[39] Chen C S, Mrksich M, Huang S, Whitesides G M and Ingber D E 1997 *Science* **276** 1425
[40] Thery M, Racine V, Piel M, Pepin A, Dimitrov A, Chen Y, Sibarita J B and Bornens M 2006 *Proc. Natl. Acad. Sci. USA* **103** 19771
[41] Maiuri P, Rupprecht J F, Wieser S, Ruprecht V, Benichou O, Carpi N, Coppey M, De Beco S, Gov N, Heisenberg C P, Crespo C L, Lautenschlaeger F, Le Berre M, Lennon-Dumenil A M, Raab M, Thiam H R, Piel M, Sixt M and Voituriez R 2015 *Cell* **161** 374
[42] Prentice-Mott H V, Meroz Y, Carlson A, Levine M A, Davidson M W, Irimia D, Charras G T, Mahadevan L and Shah J V 2016 *Proc. Natl. Acad. Sci. USA* **113** 1267
[43] Caballero D, Voituriez R and Riveline D 2014 *Biophys. J.* **107** 34
[44] Mahmud G, Campbell C J, Bishop K J M, Komarova Y A, Chaga O, Soh S, Huda S, Kandere-Grzybowska K and Grzybowski B A 2009 *Nat. Phys.* **5** 606
[45] Lautscham L A, Kammerer C, Lange J R, Kolb T, Mark C, Schilling A, Strissel P L, Strick R, Gluth C, Rowat A C, Metzner C and Fabry B 2015 *Biophys. J.* **109** 900
[46] Metzner C, Mark C, Steinwachs J, Lautscham L, Stadler F and Fabry B 2015 *Nat. Commun.* **7516** 8
[47] Bruckner D B, Fink A, Schreiber C, Rottgermann P J F, Radler J O and Broedersz C P 2019 *Nat. Phys.* **15** 595
[48] Brückner David B, Fink Alexandra, Radler J O and Broedersz C P 2020 *J. R. Soc. Interface* **17**
[49] Vestergaard C L, Pedersen J N, Mortensen K I and Flyvbjerg H 2015 *Eur. Phys. J. Special Topics* **224** 1151
[50] Liu Y, Jiao Y, Fan Q, Zheng Y, Li G, Yao J, Wang G, Lou S, Chen G, Shuai J and Liu L 2021 *Biophys. J.* **120** 2552
[51] Liu Y, Jiao Y, He D, Fan Q, Zheng Y, Li G, Wang G, Yao J, Chen G, Lou S, Shuai J and Liu L 2021 *Phys. Bio.* **18** 046007
[52] Charras G and Sahai E 2014 *Nature Reviews Molecular Cell Biology* **15** 813
[53] Novikova E A, Raab M, Discher D E and Storm C 2017 *Phys. Rev. Lett.* **078103** 5

[54] Liang L, Jones C, Chen S H, Sun B and Jiao Y 2016 *Phys. Bio.* **066001** 11
[55] Nan H Q, Liang L, Chen G, Liu L Y, Liu R C and Jiao Y 2018 *Phys. Rev. E* **033311** 13
[56] Nan H Q, Zheng Y, Lin Y H H, Chen S H, Eddy C Z, Tian J X, Xu W X, Sun B and Jiao Y 2019 *Soft Matter* **15** 6938
[57] Zheng Y, Nan H, Liu Y P, Fan Q H, Wang X C, Liu R C, Liu L Y, Ye F F, Sun B and Jiao Y 2019 *Phys. Rev. E* **043303** 13
[58] Zheng Y, Fan Q H, Eddy C Z, Wang X C, Sun B, Ye F F and Jiao Y 2020 *Phys. Rev. E* **102** 052409
[59] Fan Q, Zheng Y, Wang X, Xie R, Ding Y, Wang B, Yu X, Lu Y, Liu L, Li Y, Li M, Zhao Y, Jiao Y and Ye F 2021 *Angewandte Chemie (International ed. in English)* **60** 11858
[60] Han W, Chen S, Yuan W, Fan Q, Tian J, Wang X, Chen L, Zhang X, Wei W, Liu R, Qu J, Jiao Y, Austin R H and Liu L 2016 *Proc. Natl. Acad. Sci. USA* **113** 11208
[61] Liu Y P, Li X, Qu J, Gao X J, He Q Z, Liu L Y, Liu R C and Shuai J W 2020 *Frontiers of Physics* **15** 13602
[62] Liu Y P, Zhang X C, Wu Y L, Liu W, Li X, Liu R C, Liu L Y and Shuai J W 2017 *Chin. Phys. B* **26** 128707
[63] Wu P H, Giri A and Wirtz D 2015 *Nature Protocols* **10** 517
[64] Jeon J H, Leijnse N, Oddershede L B and Metzler R 2013 *New J. Phys.* **15** 045011
[65] Pedersen J N, Li L, Gradinaru C, Austin R H, Cox E C and Flyvbjerg H 2016 *Phys. Rev. E* **94** 062401